American Society of Hematology
2021 L Street NW, Suite 900,
Washington, DC 20036
Phone: 202-776-0544 | Fax 202-776-0545
editorial@hematology.org

Translational Regulation of Sf1 Integrates Alternative Splicing and Hematopoietic Stem Cell Fate

Tracking no: BLD-2025-032484R1

Vladyslava Liudkovska (IMol Polish Academy of Sciences, Poland) Martyna Ciołek (IMol PAN, Poland) Daniel Grygorowicz (IMol PAN, Poland) Ankita Kumari (IMol PAN, Poland) Sandra Binias (Nencki Institute of Experimental Biology, Polish Academy of Sciences, Poland) Jan Mikołajczyk (Institute of Biochemistry and Biophysics Polish Academy of Sciences, Warsaw, Poland, Poland) Anna Lenkiewicz (Nencki Institute of Experimental Biology, Polish Academy of Sciences, Poland) Anna Konturek-Ciesla (D-BSSE ETH Zurich, Switzerland) Agata Szade (Jagiellonian University, Poland) Bartosz Wojtas (Nencki Institute of Experimental Biology, Polish Academy of Sciences, Poland) Remigiusz Serwa (IMol PAN, Poland) Tomasz Turowski (Institute of Biochemistry and Biophysics Polish Academy of Sciences, Warsaw, Poland, Poland) David Bryder (Lund University, Sweden) Krzysztof Szade (Jagiellonian University, Faculty of Biochemistry, Biophysics and Biotechnology, Poland) Maciej Ciesla (IMol Polish Academy of Sciences, Poland)

Abstract:
The transition of hematopoietic stem cells (HSCs) from quiescence to lineage commitment requires precise post-transcriptional control, yet the contribution of mRNA isoform regulation remains poorly defined. Here, we identify a translationally controlled splicing program that contributes to HSC fate decisions. Using activity-based signatures of 305 splicing regulators, we uncover widespread post-transcriptional modulation of the spliceosome in stem and progenitor cells. The branch-point recognition factor Sf1 emerges as a key node, regulated by a conserved structured 5′ UTR that cooperates with the RNA-binding protein Igf2bp2 to control its translation. Disrupting this cis-trans module reduces Sf1 protein synthesis and skews differentiation toward stem and erythroid programs. Mechanistically, Sf1-dependent alternative splicing remodels 5′ UTRs of hematopoietic and DNA damage response genes, altering their translation and modulating DNA damage resolution. Together, these findings reveal an unrecognized translational layer controlling spliceosome activity and link RNA regulons, alternative splicing, and HSC fate determination.

Conflict of interest: No COI declared

COI notes:

Preprint server: No;

Author contributions and disclosures: Conceptualization, M.Cie.; Methodology, M.Cie., V.L. and M.Cio.; Investigation, V.L., A.K., A. S., D.G., J.M., A.M.L., A.K.C., T.T, K.S. and M.Cie.; Resources, V.L., A.K.C., and D.B.; Software, M.Cio. and V.L.; Formal Analysis, M.Cie., V.L., M.Cio., S.B. and B.W.; Data Curation, V. L., R.S., T.T and M.Cio. Writing - Original Draft, M.Cie.; Writing - Review & Editing, M.Cie., D. B. and V. L., with feedback from all Authors; Supervision, M.Cie.; Project Administration, M.Cie.; Funding acquisition, M.Cie.

Non-author contributions and disclosures: No;

Agreement to Share Publication-Related Data and Data Sharing Statement: Further information and requests for resources should be directed to and will be fulfilled by the Lead Contact, Maciej Cieśla (m.ciesla@imol.institute). Materials availability All unique and stable reagents generated in this study are available from the lead contact upon completion of a Materials Transfer Agreement (MTA). Data and code availability RNA sequencing data (bulk RNA-seq and single-cell RNA-seq with CITE-seq) have been deposited in the Gene Expression Omnibus (GEO) database (https://www.ncbi.nlm.nih.gov/geo/) under the following accession numbers: GSE294393 and GSE295107.

Clinical trial registration information (if any):

Translational Regulation of Sf1 Integrates Alternative Splicing and Hematopoietic Stem Cell Fate

Vladyslava Liudkovska[1], Martyna Ciołek[1], Daniel Grygorowicz[1], Ankita Kumari[1], Sandra Binias[2], Jan Mikołajczyk[3], Anna M. Lenkiewicz[4], Anna Konturek-Cieśla[5,6], Agata Szade[7], Bartosz Wojtas[2], Remigiusz Serwa[1], Tomasz Turowski[3], David Bryder[6], Krzysztof Szade[8], and Maciej Cieśla[1,*]

[1]IMol Polish Academy of Sciences, Warsaw, Poland.

[2]Laboratory of Sequencing, Nencki Institute of Experimental Biology, Polish Academy of Sciences, Warsaw, Poland.

[3]Institute of Biochemistry and Biophysics Polish Academy of Sciences, Warsaw, Poland

[4]Laboratory of Molecular Neurobiology, Nencki Institute of Experimental Biology, Polish Academy of Sciences, Warsaw, Poland.

[5]Department of Biosystems Science and Engineering, ETH Zurich, Basel, Switzerland.

[6]Division of Molecular Hematology, Lund Stem Cell Center, Department of Laboratory Medicine, Lund University, Lund, Sweden.

[7]Department of Medical Biotechnology, Faculty of Biochemistry, Biophysics and Biotechnology, Jagiellonian University, Kraków, Poland.

[8]Laboratory of Stem Cell Biology, Faculty of Biochemistry, Biophysics and Biotechnology, Jagiellonian University, Kraków, Poland.

*Corresponding Author: Maciej Cieśla (m.ciesla@imol.institute)

Data sharing

Unique reagents are available from the corresponding author (M. Cieśla, m.ciesla@imol.institute) under a material transfer agreement. Sequencing data have been deposited in GEO under accession numbers GEO: GSE294393, GSE295107. Proteomic datasets are deposited under PRIDE accession number PXD070098.

KEY POINTS

1. Translational control of Sf1 regulates alternative splicing programs during hematopoietic differentiation.

2. Sf1-dependent splicing alters translation and DNA damage response pathways in hematopoietic stem and progenitor cells.

ABSTRACT

The transition of hematopoietic stem cells (HSCs) from quiescence to lineage commitment requires precise post-transcriptional control, yet the contribution of mRNA isoform regulation remains poorly defined. Here, we identify a translationally controlled splicing program that contributes to HSC fate decisions. Using activity-based signatures of 305 splicing regulators, we uncover widespread post-transcriptional modulation of the spliceosome in stem and progenitor cells. The branch-point recognition factor Sf1 emerges as a key node, regulated by a conserved structured 5′ UTR that cooperates with the RNA-binding protein Igf2bp2 to control its translation. Disrupting this *cis-trans* module reduces Sf1 protein synthesis and skews differentiation toward stem and erythroid programs. Mechanistically, Sf1-dependent alternative splicing remodels 5′ UTRs of hematopoietic and DNA damage response genes, altering their translation and modulating DNA damage resolution. Together, these findings reveal an unrecognized translational layer controlling spliceosome activity and link RNA regulons, alternative splicing, and HSC fate determination.

INTRODUCTION

Hematopoietic stem cells (HSCs) sustain lifelong blood production through self-renewal and multilineage differentiation[1-3]. Although functional assays and single-cell transcriptomics have refined hematopoietic lineage mapping, transcript abundance alone incompletely captures early hematopoietic stem and progenitor cell (HSPC) identity and isoform complexity[2,4-12]. These observations suggest that post-transcriptional mechanisms, including splicing and translation, contribute to HSPC fate regulation.

Alternative splicing (AS) increases the number of mRNA isoforms produced from a single gene[13,14]. This way, AS enhances the diversity of the transcriptome and allows for the spatiotemporal regulation of gene expression. The spliceosome, a multi-subunit complex composed of small nuclear RNAs (U1, U2, U4, U5, and U6) and hundreds of splicing factors (SFs), orchestrates two transesterification steps during splicing through regulated conformational rearrangements[15]. Through the formation of E, A, B, Bact, B*, and C intermediates, splicing leads to the exclusion of non-coding introns and the ligation of flanking

exons. Splicing alterations and recurrent mutations in spliceosome constituents are common in disease[16-18]. They particularly impact the blood, leading to bone marrow dysplasia and leukemia[19-23]. Our previous findings demonstrated that the abundance of individual splicing factors is regulated at the level of mRNA translation, influencing malignant progression in hematopoiesis[24]. We observe that translation of selected splicing factors is regulated through the *cis*-acting regulatory RNA motifs and structures positioned within 5′ untranslated regions (5′ UTRs). These elements guide the recognition of 5′ UTRs by specific RNA-binding proteins. However, how splicing and translation intersect to regulate hematopoietic lineage commitment and specialization under homeostasis remains unknown.

Here, we investigate how translational control of splicing factors shapes hematopoietic differentiation, focusing on circuits that govern post-transcriptional shifts in splicing factor expression.

METHODS

Detailed protocols, buffer compositions, primer sequences, and bioinformatic parameters are provided in Supplementary Methods and Table S7. Transplantation was approved by the Ethical Committee of Jagiellonian University in Kraków granted to Dr. Krzysztof Szade.

Primary HSPC isolation and cell culture

Primary HSPCs were isolated from 2- to 3-month-old C57BL/6 mice, enriched for cKit$^+$ cells by MACS, and plated on fibronectin-coated 96-well plates in PVA-based HSC expansion medium (F-12 + ITS-X + 1 mg/mL PVA + 10 ng/mL SCF + 100 ng/mL TPO) [25,26]. Human cord-blood derived CD34$^+$ HSPCs were subjected to expansion for 7 days (SFEM II with 50 ng/ml SCF, 10 ng/ml IL3, 50 ng/ml FLT3 and 20 ng/ml TPO), followed by 7 days of phase I (SFEM II with 50 ng/ml SCF, 10 ng/ml IL3, and 2U/ml EPO) and 7 days of phase II (SFEM II with 30% heat-inactivated FBS, 0.3mg/ml Holo-Transferrin, and 3U/ml EPO) erythroid differentiation (Figure 5K). NIH3T3 cells were maintained in DMEM with 10% FBS and 1% penicillin/streptomycin.

Genetic perturbations

For siRNA-mediated knockdown, cKit$^+$ HSPCs were transfected with 4 pmol Sf1-targeting or control siRNA (ON-TARGETplus SMARTpool; Dharmacon) using Lipofectamine RNAiMAX on day 0, with transfection repeated every other day until day 8. Knockdown was validated by RT-qPCR.

For CRISPR-Cas9-mediated *Sf1* 5′ UTR editing, guide RNAs were designed via IDT CRISPR-Cas9 Design Checker (Table S7) and assembled into RNPs with the Alt-R CRISPR/Cas9 kit.

HSPCs were nucleofected with the P3 Primary Cell 4D-X Kit (DS-130 program; Lonza), and NIH3T3 cells with custom buffer (U-030, Amaxa II) [24,27]. Editing efficiency was confirmed by Sanger sequencing of the targeted region. NIH3T3 proliferation and cell death following editing were assessed by crystal violet staining.

RNA isolation and RT-qPCR

Total RNA was isolated using the Direct-zol RNA Microprep Kit (Zymo Research) with on-column DNase I treatment. Reverse transcription was performed with the High-Capacity cDNA Reverse Transcription Kit (Thermo Fisher) using random hexamer primers. Real-time qPCR was performed using LightCycler® 480 SYBR Green I Master on a LightCycler® 480 II instrument (Roche). Primers are listed in Table S7.

Flow cytometry

Intracellular flow cytometry for splicing factor expression was performed on whole bone marrow co-stained for HSC surface markers, fixed in 1% PFA, permeabilized with 0.1% saponin, and stained with antibodies against Sf1, Sf3a1/2/3, Sf3b1/3/4, U2af1, Ddx42, and Ddx46 (Table S8), followed by an Alexa Fluor 594 secondary antibody.

For HSPC immunophenotyping after 8 days of ex vivo expansion**,** cells were stained for Lineage markers (B220, CD3ε, Ter119, Mac1, Gr1), cKit, Sca1, CD48, CD150, and 7-AAD. Data were acquired on a BD LSRFortessa™ and analyzed with FlowJo.

Western blotting

Cells were lysed in RIPA buffer with protease inhibitors, and quantified. Equal protein amounts (10–50 µg) were subjected to SDS-PAGE and transferred to PVDF membranes[28]. Antibodies are listed in Table S8.

Immunofluorescence

Sf1 5′ UTR del(51-100) or control NIH3T3 cells were fixed in 4% formaldehyde, permeabilized with 0.1% Triton X-100, and blocked in 3% BSA. Cells were incubated with γ-H2A.X (Ser139) primary antibody overnight, followed by Alexa Fluor 488 secondary antibody. Slides were mounted with ProLong™ Gold and imaged on a Zeiss LSM 780 confocal microscope.

Colony forming unit (CFU) assay

1×10^3 primary $cKit^+$ cells were nucleofected with Sf1-targeting or control siRNA or Cas9-gRNA RNPs and plated in MethoCult™ GF M3434 methylcellulose (35 mm dish). Colonies were scored and classified by colony type after 10–14 days. For cytological analysis, dissociated

colonies (5×10⁴ cells) were settled on slides, fixed in ethanol, and stained with May–Grünwald-Giemsa. Images were acquired on a Zeiss Axio Observer microscope.

HSPCs transplantation

cKit⁺ HSPCs from multiple (n = 3) 2- to 3-month-old mice were nucleofected with control or Sf1 5′ UTR (51-100 nt)-targeting CRISPR-Cas9 RNPs with DS130 program (Lonza) and expanded for 14 days. Lethally irradiated (900 cGy) CD45.1 recipients (n = 5-7 per group) were transplanted via retro-orbital injection with 5×10⁴ HSPCs (CD45.2) plus 3×10^5 CD45.1 bone marrow support cells. Peripheral blood chimerism was assessed by flow cytometry (CD45.2/CD45.1 ratios) in combination with lineage markers (CD3, B220, Ly6C, Ly6G) at 4-, 8-, 12-, and 16-weeks post-transplantation. Detailed protocol in Supplementary Methods.

Luciferase assay

Full-length (398 nt) murine *Sf1* 5′ UTR[29] and serial 50-nt deletion mutants were cloned into a monocistronic firefly luciferase reporter. To disrupt the predicted RNA secondary structures, we introduced transverse mutations in the base-pairing regions of stem-loops 2 and 3, replacing complementary nucleotides with non-pairing bases (e.g., A-T to A-A). NIH3T3 cells were transfected with 1 µg plasmid, harvested after 48 h, and luciferase activity was measured (Promega Luciferase Reporter Assay System).

Polysome fractionation

Polysome fractionation was performed as described[30-32]. NIH3T3 cells, or HSPCs nucleofected with Sf1 5′ UTR (51-100 nt) gRNAs and expanded for 14 days, were treated with 10 µg/mL cycloheximide (CHX), lysed in polysome buffer, and layered on 10–50% sucrose gradients. Following ultracentrifugation, gradients were fractionated; transcript distribution was analyzed with RT-qPCR. Full protocol in Supplementary Methods.

Sf1 5′ UTR RNA pulldown and proteomics

To identify proteins binding the Sf1 5′ UTR, we used the MS2 tethering system[33]. NIH3T3 cells stably expressing WT or del(51-100) Sf1 5′ UTR-Fluc reporters carrying MS2 stem loops were transfected with a FLAG-tagged MS2-coat protein fusion (FLAG-NLS-MS2-GFP) [33], which captures the MS2-tagged reporter RNA in cells. Cells were UV-crosslinked, lysed, and the FLAG-MS2-RNA-protein complexes were immunoprecipitated with anti-FLAG M2 magnetic beads (Sigma). Eluted proteins were reduced, alkylated, trypsin-digested, desalted, TMT-labeled, and analyzed by nano-LC–MS/MS on a Q Exactive HF-X. Data were processed with MaxQuant v2.6.7.0[34, 35] and Perseus v1.6.10[36]. Differential enrichment of bound proteins was determined by comparing WT and del(51-100) pulldowns to non-transfected cells (Table S1). Full protocol in Supplementary Methods.

RNA Immunoprecipitation

Confluent NIH3T3 cells (n = 6) stably expressing the WT Sf1 5′ UTR–Fluc reporter (FL), the Δ51–100 nt mutant (MUT), or non-transfected controls (WT) (n = 3 biological replicates per condition) were UV-crosslinked (254 nm, 400 mJ/cm²), lysed, and incubated with 3.4 µg anti-Igf2bp2 (D4R2F, CST #14672) for 2h at 4°C, followed by overnight capture on Dynabeads Protein A (Thermo Fisher). Per-condition pooled no-antibody controls were processed in parallel. After washes and Proteinase K digestion, RNA was isolated and reverse transcribed. RT-qPCR was analyzed as IP/Total ratio = $2^{Ct\_Total - Ct\_IP}$, which controls for differences in transcript abundance between conditions. Detailed protocol in Supplementary Methods.

CLIP-seq

CLIP was performed on UV-crosslinked NIH3T3 cells (254 nm, 400 mJ/cm²; n = 3 biological replicates plus a non-crosslinked control). Cells were lysed, cleared, and Igf2bp2-RNA complexes were immunoprecipitated overnight with anti-Igf2bp2 (D4R2F, CST #14672; 10 µg per sample) on Dynabeads Protein A. On-bead partial RNase digestion (RNace-IT) was followed by 3′ adapter ligation, T4 PNK 5′ phosphorylation and ^{32}P radiolabeling, and 5′ barcoded adapter ligation. Cross-linked Igf2bp2-RNA complexes were resolved by Bis-Tris SDS-PAGE, transferred to nitrocellulose, visualized by autoradiography, and the corresponding region was excised. RNA was recovered by Proteinase K digestion and phenol-chloroform extraction, reverse-transcribed (SuperScript IV), PCR-amplified with indexed primers, and sequenced on an Illumina platform. Reads were processed using a custom CLIP pipeline incorporating FASTX-Collapser, Flexbar[37], and STAR (GRCm39) [38]. Coverage tracks were generated with deepTools (bamCoverage) [39]. Downstream analyses used the trxtools v0.5.0 package (https://github.com/TurowskiLab/trxtools[40]) and custom Python scripts. Detailed protocol in Supplementary Methods.

Splicing Factor Signatures in Human Hematopoietic Cells

Custom splicing factor signatures were derived from published transcriptomic datasets[41] and applied to hematopoietic populations in bone marrow, blood and lymph node from the Tabula Sapiens atlas[42]. Signature activity was computed as weighted gene expression sums normalized to background, visualized as z-scored heatmaps, and compared to mRNA expression by Pearson correlation, with statistical testing via Wilcoxon rank-sum and BH correction. Analyses used Scanpy (Python), edgeR/limma/Seurat (R); details in Supplementary Methods.

RNA-sequencing and splicing analysis

Control or Sf1 del(51-100) HSPCs expanded for 21 days were used for transcriptome analysis. Libraries were prepared from total RNA using the KAPA RNA HyperPrep kit with RiboErase (Roche), and sequenced on NovaSeq 6000 (2×101 bp). Reads were adapter-trimmed (Skewer) [43], quality-checked (FastQC), aligned to GRCm39 (STAR) [38], and gene-level counts obtained with featureCounts. Differential gene expression was analyzed with DESeq2 (batch-corrected) [44]. Differential alternative splicing events (SE, A5SS, A3SS, RI, MXE) were identified using rMATS Turbo v4.3.0[45] (FDR <0.05, ΔPSI ≥0.1, read count ≥10). GO analysis was performed using Enrichr. RBP motif enrichment in Sf1-regulated exons was assessed using CISBP-RNA[46] within the standard proximal splicing regulatory window used in Matt analyses (±35 nt exonic, ±135 nt intronic around splice junctions). Exons with increased inclusion (UP), decreased inclusion (DOWN), or unchanged (NO) were compared. Sequence features were analyzed using Matt[47] (Tables S4-S6).

Single-cell (sc)RNA sequencing with CITE-seq

HSPCs expanded for 21 days were pooled (CTRL, del(51-100), del(251-300)), filtered, counted, and loaded on 10x Genomics Chromium chips in quadruplicate. Libraries were prepared with the 3′ Next GEM kit (Feature Barcoding), QCed on Bioanalyzer, and sequenced on NovaSeq 6000 (target depth 4×10^4 mRNA + 7×10^3 Ab-oligo reads per cell). CITE-seq hashing was used exclusively for multiplexing and discrimination of pooled CTRL, del(51-100), and del(251-300) HSPC samples in scRNA-seq. FASTQ files were processed with Cell Ranger v7.2.0. Demultiplexed h5 objects were analyzed in Seurat (v4.4) [48], filtered for quality, normalized with CLR or SCTransform, clustered (resolution 0.2), and marker genes identified. Detailed protocol in Supplementary Methods.

Quantification and statistics

Data are shown as mean ± SD or SEM; replicates and statistical tests are indicated in figure legends.

RESULTS

Splicing Factor Activity Signatures reveal Post-transcriptional Regulation of the Spliceosome during Hematopoietic Differentiation

HSPCs display phenotypic properties incompletely explained by steady-state transcriptomes, suggesting important post-transcriptional regulation of stemness. In particular, HSPCs rely on translation and splicing, with disruptions in either process linked to hematologic malignancies, including myelodysplastic syndromes and leukemia[20,49-52].

To interrogate spliceosome regulation across hematopoiesis, we constructed activity signatures for 305 SFs based on transcriptomic responses to SF perturbations as proxies for protein-level activity[41] (Fig. 1A, S1A). We applied these signatures to the Tabula Sapiens atlas across hematopoietic tissues, enabling quantitative mapping of SF activity[42].

This analysis revealed differences in inferred SF activity across hematopoiesis (Fig. 1B, S1B). Erythroid cells displayed globally elevated signature scores, consistent with reduced splicing demand in transcriptionally attenuated states. In contrast, bone marrow populations showed marked heterogeneity in SF activity, suggesting remodeling of spliceosomal programs during hematopoietic differentiation.

SF activity segregated into lineage-associated clusters across hematopoiesis (Fig. 1C, S1C). HSCs showed relatively higher inferred activity of U4/U6 tri-snRNP and minor spliceosome (U11/U12) components, whereas early progenitors were enriched for SR proteins and second-step factors, including Prp19-associated complexes. Differentiated populations such as B cells exhibited elevated activity across multiple SF families (negative signature scores), consistent with coordinated activation of spliceosomal modules.

Unsupervised clustering of SF activity profiles further revealed coherent groups of SFs with lineage-dependent dynamics (Fig. 1D). These clusters were not explained by SF mRNA abundance, indicating that activity-based regulation is decoupled from transcriptional output.

These analyses indicate that SF regulation is progressively reconfigured during hematopoietic differentiation rather than undergoing discrete, lineage-restricted switching of individual factors (Fig. 1E, S1D), consistent with coordinated remodeling of spliceosomal programs across hematopoietic states.

Dynamics in Splicing Factors Define Hematopoietic Lineage Trajectories

To validate the computational predictions in primary cells, we revisited published ultra-low-input ribosome profiling datasets of early hematopoietic differentiation[53]. This analysis revealed translational regulation of core spliceosomal components, whereas auxiliary splicing factors remained largely unchanged (Fig. 2A). To validate this at the protein level, we employed intracellular flow cytometry (icFlow) to quantify splicing factors involved in the first catalytic step of splicing, during which branch point (BP) recognition and splice site fidelity are established (Fig. 2B and S2A). Our analysis of protein levels across hematopoietic ontogeny by icFlow, juxtaposed with available mRNA datasets (https://gexc.riken.jp/)[54], uncovered a striking discordance. While the mRNA levels of core splicing factors remained stable, their protein expression exhibited lineage-specific variations (Fig. 2C, D, and S2B).

For instance, splicing factors from the Sf3 family of the U2 snRNP showed a modest protein-level increase in early progenitors, followed by lineage-specific divergence: their expression decreased in lymphoid cells (Lin^+, SSC/FSC^{low}), but was elevated in myeloid population (Lin^+, SSC^{high}) (Fig. 2C). Instead, Sf1, a key factor recognizing the branch point adenosine (BPA) [55], was transiently upregulated at the multipotent progenitor (MPP, $Lin^-c\text{-}Kit^+Sca\text{-}1^+CD48^+CD150^-$) stage, following HSC exit from quiescence, before returning to basal levels, suggesting a role in early hematopoietic activation.

Notably, while some splicing factors exhibited protein expression patterns that aligned with established surface markers, others displayed a bimodal distribution within individual populations (Fig. 2D and S2B). Sf1 serves as a prime example, displaying heterogeneous expression within the MPP and granulocyte-monocyte-lymphoid progenitors (GMLP, LSK $CD150^-CD48^+$) populations (Fig. 2D).

To functionally interrogate these dynamic expression patterns, we employed an *ex vivo* HSC expansion system[25,26], coupled with RNA interference-mediated knockdown of candidate splicing factors (Fig. 2E and S2C). While depletion of most splicing factors resulted in reduced cell numbers, consistent with their essential roles in homeostasis, knockdown of Sf1 and the core Sf3a component Sf3a3 increased the stem cell-enriched $CD150^+$ LSK fraction, suggesting their role in stem cell maintenance rather than viability (Fig. 2E). Further immunophenotypic analysis following Sf1 knockdown revealed a partial loss of LSKs, accompanied by an accumulation of $CD150^+$ LSKs (Fig. 2F, G). Functionally, Sf1 depletion impaired colony-forming capacity and led to accumulation of morphologically immature cells with high nucleus-to-cytoplasm ratios, consistent with impaired differentiation and retention of stem-like features (Fig. 2H, I).

Together, these findings demonstrate that post-transcriptional regulation of splicing factors contributes to early HSPC fate decisions, with Sf1 required for proper hematopoietic differentiation.

Sf1 Expression is Translationally Controlled via a Structured 5′ UTR Regulatory Element

To elucidate the mechanisms underlying Sf1 expression and the discordance between its mRNA and protein levels during hematopoietic differentiation, we investigated post-transcriptional control, focusing on translation initiation. This process, governed by ribosomal scanning through the 5′ UTR with initiation factors, is a critical checkpoint in protein synthesis[56,57]. Beyond these mechanisms, *cis*-regulatory structural and sequence elements within 5′ UTRs can modulate translation efficiency[56].

Analysis of the Sf1 genomic locus identified four predicted 5′ UTR isoforms, with the longest spanning 398 nucleotides (nt) (Fig. 3A and S3A). This extended 5′ UTR is highly conserved across mammals (Fig. 3A and S3A, B), with enrichment in the proximal segment where RNA secondary structure predictions identified stable stem-loop structures (SL1–SL3) with favorable folding energy scores (Fig. 3B, S3B).

To determine the impact of the Sf1 5′ UTR on translation, we generated deletions across its 398-nt sequence using a monocistronic translational reporter, removing 50-nt segments (Fig. 3C). This identified the 51–100 nt region as a major contributor to translational activity, with its removal reducing reporter expression. Notably, this region overlaps conserved SL2 and SL3 structural elements (Fig. 3B, D). Using mutate-and-map analysis, we identified SL2 as a minimal element required for efficient translation, as its disruption impaired reporter activity (Fig. 3E).

To assess the physiological relevance of this mechanism, we introduced deletions in the Sf1 5′ UTR using CRISPR-Cas9 in murine fibroblasts. In line with our reporter assays, deletions spanning nucleotides 51–200 reduced Sf1 protein without affecting mRNA levels (Fig. 3F and S3C). Cells carrying these deletions exhibited reduced viability and proliferation, suggesting that translational control of Sf1 is essential for cellular fitness (Fig. S3D).

Extending these findings to primary HSPCs, we used CRISPR-Cas9 to delete nucleotides 51–100 of the 5′ UTR (del(51-100)), which reduced Sf1 protein expression without affecting transcript levels (Fig. 3G). Polysome profiling of del(51-100) cells revealed a shift of *Sf1* mRNA toward lighter fractions, consistent with reduced translational efficiency rather than altered protein stability (Fig. 3H).

Collectively, our results identify a conserved, structured 5′ UTR element as a determinant of *Sf1* translation, revealing a post-transcriptional regulatory circuit that fine-tunes Sf1 abundance.

Sf1 Translation Requires a Cooperativity between *Cis*-Acting Stem-Loop2 and Igf2bp2-Mediated Regulation

Having established that Sf1 expression is controlled by a conserved 5′UTR element (Fig. 3), we next tested whether its regulation depends on cooperation between cis-regulatory RNA structure and trans-acting RNA-binding proteins. Structured 5′ UTRs often serve as platforms for translational regulators, suggesting a mechanism for Sf1 control.

To identify candidate factors, we performed quantitative proteomics of RNA pulldowns from NIH3T3 cells expressing either the WT or a del(51-100) Sf1 5′UTR mutant. TMT analysis revealed proteins enriched on the WT 5′UTR, consistent with this region acting as a

translational regulatory hub (Fig. 4A, Table S1). Among these, Igf2bp2 emerged as a top candidate, consistent with its role in promoting translation via recruitment of the eIF4A1 complex[58,59]. Accordingly, CLIP-seq showed Igf2bp2 binding to Sf1 mRNA, with an enrichment peak in the 5′UTR ~200 nt downstream of the TSS (Fig. 4B and S4A, B). While Igf2bp2 is a known m^{6}A reader[60], no canonical RRACH motif was identified within the Sf1 5′UTR, suggesting that Igf2bp2 binding may depend on alternative sequence or structural RNA features rather than canonical m^{6}A recognition.

We next tested whether Igf2bp2 regulates *Sf1* translation using luciferase reporters containing WT or mutant *Sf1* 5′UTRs. WT reporters were sensitive to Igf2bp2 depletion, whereas mutants disrupting the 51–100 region or SL2 structure were largely unresponsive, indicating that this *cis*-element is required for Igf2bp2-dependent translational activation (Fig. 4C). Consistent with this, Igf2bp2 knockdown reduced Sf1 protein levels without affecting mRNA in NIH3T3 cells (Fig. 4D, S4C) and primary HSPCs (Fig. 4E).

Polysome profiling confirmed translational regulation: Igf2bp2 depletion shifted *Sf1* mRNA to lighter polysome fractions, indicating reduced ribosome loading (Fig. 4F,G). Functionally, Igf2bp2 knockdown phenocopied *Sf1* depletion in murine HSPCs (Fig. 2G), increasing the CD150$^+$ LSK fraction (Fig. 4H).

Together, these findings support a model in which a structured stem-loop within the *Sf1* 5′UTR recruits Igf2bp2 to enhance translation initiation, linking *cis*-regulatory RNA architecture to post-transcriptional control of splicing factor abundance and HSPC state transitions.

Loss of Translational Control of Sf1 Alters HSC Fate and Enhances Stem Cell Potential

To investigate the physiological consequences of disrupted Sf1 translation in HSPCs, we compared control and del(51-100) cells under conditions supporting stem maintenance or differentiation. del(51-100) cells displayed an increased proportion of CD150$^+$ LSK cells (Fig. S5A), consistent with accumulation of immunophenotypically primitive HSPCs. In parallel, these cells showed reduced colony formation under differentiation-promoting conditions, suggesting impaired lineage commitment (Fig. S5B).

To resolve these state shifts at single-cell resolution, we performed scRNA-seq on expanded control and del(51-100) HSPCs (41,515 cells). Unsupervised clustering identified seven transcriptionally distinct populations corresponding to stem-like, myeloid-primed, lymphoid, and megakaryocyte/erythroid states (Fig. 5A, B, S5C). The del(51-100) cells were depleted from myeloid-primed cluster 1 and enriched in cluster 2 (stem-like) as well as megakaryocyte/erythroid-associated clusters 4 and 7, indicating a shift toward primitive and MEP-like states (Fig. 5C, S5C).

We next assessed differential gene expression within each cluster between control and del(51-100) cells. This revealed largely non-overlapping gene programs across clusters (Fig. 5D, Table S2), indicating that Sf1 translation affects cell-state-specific transcriptional outputs. Notably, the most affected cluster 2 (stem-like) and cluster 4 (megakaryocyte/erythroid), showed enrichment for pathways implicated in stem cell maintenance and hematopoietic regulation, including PI3K signaling[61,62], heparan sulfate biosynthesis[63,64], and metabolic and chromatin-associated processes such as Na^+ binding[65] and H3K36 demethylase regulation[66,67].

Consistently, GO analysis of differentially expressed genes highlighted enrichment of pathways linked to hematopoietic differentiation, chromatin regulation, and myeloid specification (Fig. 5E, S5D, E, Table S4), supporting rewiring of lineage-associated programs.

To assess functional consequences, we performed serial replating assays. The del(51-100) HSPCs retained colony-forming capacity upon replating and were characterized by maintained erythroid outputs, with drops in myeloid lineages (Fig. 5F, G), consistent with sustained self-renewal-like properties and high erythroid differentiation capacity. During erythroid differentiation, SF1 knockdown increased cell expansion and transiently enriched erythroid populations (Fig. 5K, L, S5G, H), indicating conserved effects on erythroid differentiation dynamics.

Finally, *in vivo* transplantation of limiting numbers of control and del(51-100) HSPCs into irradiated recipients revealed enhanced long-term engraftment and increased donor-derived hematopoiesis in del(51-100) conditions, with early and sustained myeloid contribution (Fig. 5H-J, S5F). Together with scRNA-seq and functional analyses, these findings indicate that loss of Sf1 translational control prolongs primitive and erythroid-associated states through altered differentiation kinetics rather than impaired lineage output, identifying Sf1 as a conserved regulator of hematopoietic state transitions across murine and human systems.

Sf1 Translation Links Alternative Splicing to Hematopoietic and Genome Stability Programs

We reasoned that perturbed translation of Sf1 would impact splicing dynamics by influencing availability of the protein required for branch point site recognition. To investigate how splicing is regulated under disrupted Sf1 translation, we examined splicing fidelity in del(51-100) HSPCs. We performed paired-end sequencing of rRNA-depleted mRNA on ex vivo expanded HSPCs with or without regulated Sf1 translation (Fig. 6A, S6A and Table S5).

rMATS[68] analyses identified ~4,000 alternative splicing events (ASEs), including exon skipping (SE), mutually exclusive exons (MXE), alternative 5′ or 3′ splice sites (alt5′ss or

alt3′ss), and intron retention (IR). Consistent with the role of Sf1 in branch point site recognition[55], del(51-100) predominantly affected SE events (Fig. 6A, B). Differentially spliced exons were enriched for features linked to alternative exon usage, including shorter branch point-to-3′ splice site distances, longer polypyrimidine tracts, and reduced predicted Sf1 binding strength (Fig. S6B-E). These exons were also preferentially flanked by long introns and GC-rich upstream exons (Fig. S6F,G). We further observed altered enrichment of U2AF2 binding sites among transcripts with decreased exon inclusion (Fig. S6H), consistent with functional coupling between Sf1 and the U2af complex[69], suggesting that Sf1 perturbation reshapes splice-site recognition within a broader regulatory network.

Splicing provides a rapid mechanism to reprogram functionally related transcripts[13,32]. In del(51-100) HSPCs, alternatively spliced transcripts were enriched for pathways linked to hematopoietic maintenance and the DNA damage response (DDR) (Fig. 6C, D), including key regulators such as *Parp2, Atr, Chek2, Rad52,* and *Atrx* (Fig. 6D, S6K). We observed a positional bias: skipped exon events were enriched within 5′UTRs, particularly among DDR-associated transcripts (odds ratio 3.1 vs. 2.7 transcriptome-wide), whereas little enrichment was seen in coding regions or 3′UTRs (Fig. 6E). This suggested Sf1-dependent splicing modulates translational control through 5′UTR remodeling.

Consistent with this, polysome profiling revealed altered ribosome association for candidate alternatively spliced transcripts (Fig. 6F and S6I), indicating that Sf1-dependent splicing can influence translation efficiency. Disruption of Sf1 translation led to modest activation of DNA damage response pathways, evidenced by increased γH2AX foci in fibroblasts (Fig. 6G) and elevated p53 levels in HSPCs (Fig. S6J).

To assess conservation, we performed SF1 knockdown in human $CD34^+$ HSPCs. SF1 depletion induced widespread splicing alterations (~8,800 events, Table S6), predominantly SE and RI (Fig. 6H), without global changes in transcript abundance (Fig. 6I). These events significantly overlapped with those in murine HSPCs (Fig. 6J) and were enriched for DDR pathways (Fig. 6K), indicating a conserved SF1-dependent splicing program.

Together, these findings identify Sf1 as a regulator of conserved splicing events that preferentially remodel 5′UTRs of functionally related transcripts, including DDR components, thereby influencing translation and genomic integrity in hematopoietic progenitors.

DISCUSSION

Fate decisions in HSCs are orchestrated through multilayered regulatory mechanisms, spanning transcriptional, translational, and splicing control. Here, we uncover an unrecognized layer of regulation in which translational control of *Sf1* dictates splicing decisions that shape

HSC differentiation and genomic stability. Our findings challenge the view of splicing as a mere housekeeping process and highlight the pivotal role of translation-dependent modulation of splicing factor expression in cell fate determination.

SF1 is a key factor in branch point recognition and spliceosome assembly[69,70], yet the physiological consequences of modulating its levels remain poorly understood. Although mammalian studies suggested modest effects of SF1 on splicing[69], and SF1 depletion in *Caenorhabditis elegans* increased the lifespan through TORC1 signaling[71], our data reveal widespread SF1-dependent splicing control in mammalian stem cells. These findings support a context-dependent role for SF1 and suggest that structured 5′ UTR-mediated translational control tunes SF1 levels to meet the splicing demands of HSCs[72-74].

The reliance of HSCs on tightly controlled splicing programs parallels observations in other specialized cell types, including neurons, where alternative splicing supports transcriptome diversification, local translation, and functional specialization[75-77]. Together, these observations suggest that specialized cells may depend disproportionately on post-transcriptional mechanisms, including splicing and translation, to achieve functional complexity.

Our findings suggest that differential levels of splicing factors, including Sf1, may contribute to rate-limiting steps in spliceosome activity and selectively influence transcripts with distinct *cis*-regulatory features. Together with studies showing that RNA-binding proteins organize membrane-less splicing compartments and locally concentrate spliceosome components[78,79], these observations raise the possibility that translational control of splicing factors helps shape cell type-specific splicing efficiency and transcript processing.

Collectively, our findings uncover a mechanism by which translational regulation of splicing factors influences hematopoietic differentiation and DNA damage resolution. The magnitude and consequences of DNA damage signaling appeared context-dependent, consistent with previous observations in hematopoietic stem cells[80,81]. These results position splicing regulation as an integral component of hematopoietic state control rather than a downstream consequence of lineage specification. Given the growing recognition of alternative splicing in disease states, dysregulated splicing programs and their downstream effectors may provide more realistic avenues for therapeutic intervention in hematologic disorders and malignancies.

ACKNOWLEDGMENTS

We thank members of the Cieśla laboratory for helpful discussion and thoughtful feedback and Magda Konarska and Cristian Bellodi for critical reading. We acknowledge expert help from the IIMCB Genome Engineering Facility and Microscopy Facility (IN-MOL-CELL Infrastructure) funded by the European Union – NextGenerationEU under the National

Recovery and Resilience Plan. IN-MOL-CELL Infrastructure was also funded by the European Union under Horizon Europe (Project 101059801 – RACE) and by RACE-PRIME project carried out within the IRAP programme of the Foundation for Polish Science co-financed by the European Union under the European Funds for Smart Economy 2021-2027 (FENG). We thank Marcin Szpila, Paweł Kożuch, Kacper Kowalski, and Patrycja Kwiecińska for expert experimental help, and acknowledge Abdelhalim Azzi for a kind gift of NIH3T3 cells. We are indebted to the Flow Cytometry Laboratory at the Nencki Institute of Polish Academy of Sciences for assistance with flow cytometry analysis. NGS was performed in the Genomics Core Facility CeNT UW (RRID:SCR_022718), using the NovaSeq 6000 platform financed by the Polish Ministry of Science and Higher Education (decision no. 6817/IA/SP/2018 of 2018-04-10). High-throughput data analysis was carried out with the support of the Interdisciplinary Centre for Mathematical and Computational Modelling, University of Warsaw (ICM UW) under computational allocations nos. g96-1870 and g101-2286. M.Cie. is a beneficiary of EMBO Installation Grant, First Team FENG.02.02-IP.05-0074/24 grant from Foundation for Polish Science, Sonata Bis (UMO-2022/46/E/NZ3/00141) and OPUS (UMO-2021/43/B/NZ3/01177) grants from National Science Center in Poland.

AUTHOR CONTRIBUTIONS

Conceptualization, M.Cie.; Methodology, M.Cie., V.L. and M.Cio.; Investigation, V.L., A.K., A. S., D.G., J.M., A.M.L., A.K.C., T.T, K.S. and M.Cie.; Resources, V.L., A.K.C., and D.B.; Software, M.Cio. and V.L.; Formal Analysis, M.Cie., V.L., M.Cio., S.B. and B.W.; Data Curation, V. L., R.S., T.T and M.Cio. Writing - Original Draft, M.Cie.; Writing – Review & Editing, M.Cie., D. B. and V. L., with feedback from all Authors; Supervision, M.Cie.; Project Administration, M.Cie.; Funding acquisition, M.Cie.

CONFLICT OF INTEREST

All Authors have not reported any conflict of interests.

REFERENCES

1. Eaves, C.J. (2015). Hematopoietic stem cells: concepts, definitions, and the new reality. Blood *125*, 2605-2613. 10.1182/blood-2014-12-570200.
2. Haas, S., Trumpp, A., and Milsom, M.D. (2018). Causes and Consequences of Hematopoietic Stem Cell Heterogeneity. Cell Stem Cell *22*, 627-638. 10.1016/j.stem.2018.04.003.
3. Laurenti, E., and Göttgens, B. (2018). From haematopoietic stem cells to complex differentiation landscapes. Nature *553*, 418-426. 10.1038/nature25022.
4. Konturek-Ciesla, A., Dhapola, P., Zhang, Q., Säwén, P., Wan, H., Karlsson, G., and Bryder, D. (2023). Temporal multimodal single-cell profiling of native hematopoiesis illuminates altered differentiation trajectories with age. Cell Rep *42*, 112304. 10.1016/j.celrep.2023.112304.
5. Velten, L., Haas, S.F., Raffel, S., Blaszkiewicz, S., Islam, S., Hennig, B.P., Hirche, C., Lutz, C., Buss, E.C., Nowak, D., et al. (2017). Human haematopoietic stem cell lineage commitment is a continuous process. Nat Cell Biol *19*, 271-281. 10.1038/ncb3493.
6. Belchikov, N., Hsu, J., Li, X.J., Jarroux, J., Hu, W., Joglekar, A., and Tilgner, H.U. (2024). Understanding isoform expression by pairing long-read sequencing with single-cell and spatial transcriptomics. Genome Res *34*, 1735-1746. 10.1101/gr.279640.124.
7. Papalexi, E., and Satija, R. (2018). Single-cell RNA sequencing to explore immune cell heterogeneity. Nat Rev Immunol *18*, 35-45. 10.1038/nri.2017.76.
8. La Manno, G., Soldatov, R., Zeisel, A., Braun, E., Hochgerner, H., Petukhov, V., Lidschreiber, K., Kastriti, M.E., Lönnerberg, P., Furlan, A., et al. (2018). RNA velocity of single cells. Nature *560*, 494-498. 10.1038/s41586-018-0414-6.
9. Chen, L., Kostadima, M., Martens, J.H.A., Canu, G., Garcia, S.P., Turro, E., Downes, K., Macaulay, I.C., Bielczyk-Maczynska, E., Coe, S., et al. (2014). Transcriptional diversity during lineage commitment of human blood progenitors. Science *345*, 1251033. 10.1126/science.1251033.
10. Ullrich, S., and Guigó, R. (2020). Dynamic changes in intron retention are tightly associated with regulation of splicing factors and proliferative activity during B-cell development. Nucleic Acids Res *48*, 1327-1340. 10.1093/nar/gkz1180.
11. Edwards, C.R., Ritchie, W., Wong, J.J., Schmitz, U., Middleton, R., An, X., Mohandas, N., Rasko, J.E., and Blobel, G.A. (2016). A dynamic intron retention program in the mammalian megakaryocyte and erythrocyte lineages. Blood *127*, e24-e34. 10.1182/blood-2016-01-692764.
12. Wong, J.J., Ritchie, W., Ebner, O.A., Selbach, M., Wong, J.W., Huang, Y., Gao, D., Pinello, N., Gonzalez, M., Baidya, K., et al. (2013). Orchestrated intron retention regulates normal granulocyte differentiation. Cell *154*, 583-595. 10.1016/j.cell.2013.06.052.
13. Ule, J., and Blencowe, B.J. (2019). Alternative Splicing Regulatory Networks: Functions, Mechanisms, and Evolution. Mol Cell *76*, 329-345. 10.1016/j.molcel.2019.09.017.
14. Kalsotra, A., and Cooper, T.A. (2011). Functional consequences of developmentally regulated alternative splicing. Nat Rev Genet *12*, 715-729. 10.1038/nrg3052.
15. Will, C.L., and Lührmann, R. (2011). Spliceosome structure and function. Cold Spring Harb Perspect Biol *3*. 10.1101/cshperspect.a003707.
16. Kahles, A., Lehmann, K.V., Toussaint, N.C., Hüser, M., Stark, S.G., Sachsenberg, T., Stegle, O., Kohlbacher, O., Sander, C., and Rätsch, G. (2018). Comprehensive Analysis of Alternative Splicing Across Tumors from 8,705 Patients. Cancer Cell *34*, 211-224.e216. 10.1016/j.ccell.2018.07.001.
17. Dvinge, H., and Bradley, R.K. (2015). Widespread intron retention diversifies most cancer transcriptomes. Genome Med *7*, 45. 10.1186/s13073-015-0168-9.
18. Scotti, M.M., and Swanson, M.S. (2016). RNA mis-splicing in disease. Nat Rev Genet *17*, 19-32. 10.1038/nrg.2015.3.

19. Yoshimi, A., Lin, K.T., Wiseman, D.H., Rahman, M.A., Pastore, A., Wang, B., Lee, S.C., Micol, J.B., Zhang, X.J., de Botton, S., et al. (2019). Coordinated alterations in RNA splicing and epigenetic regulation drive leukaemogenesis. Nature *574*, 273-277. 10.1038/s41586-019-1618-0.
20. Joshi, P., Halene, S., and Abdel-Wahab, O. (2017). How do messenger RNA splicing alterations drive myelodysplasia? Blood *129*, 2465-2470. 10.1182/blood-2017-02-692715.
21. Yoshida, K., Sanada, M., Shiraishi, Y., Nowak, D., Nagata, Y., Yamamoto, R., Sato, Y., Sato-Otsubo, A., Kon, A., Nagasaki, M., et al. (2011). Frequent pathway mutations of splicing machinery in myelodysplasia. Nature *478*, 64-69. 10.1038/nature10496.
22. Chen, S., Benbarche, S., and Abdel-Wahab, O. (2021). Splicing factor mutations in hematologic malignancies. Blood *138*, 599-612. 10.1182/blood.2019004260.
23. Saez, B., Walter, M.J., and Graubert, T.A. (2017). Splicing factor gene mutations in hematologic malignancies. Blood *129*, 1260-1269. 10.1182/blood-2016-10-692400.
24. Cieśla, M., Ngoc, P.C.T., Muthukumar, S., Todisco, G., Madej, M., Fritz, H., Dimitriou, M., Incarnato, D., Hellström-Lindberg, E., and Bellodi, C. (2023). m(6)A-driven SF3B1 translation control steers splicing to direct genome integrity and leukemogenesis. Mol Cell *83*, 1165-1179.e1111. 10.1016/j.molcel.2023.02.024.
25. Wilkinson, A.C., Ishida, R., Kikuchi, M., Sudo, K., Morita, M., Crisostomo, R.V., Yamamoto, R., Loh, K.M., Nakamura, Y., Watanabe, M., et al. (2019). Long-term ex vivo haematopoietic-stem-cell expansion allows nonconditioned transplantation. Nature *571*, 117-121. 10.1038/s41586-019-1244-x.
26. Wilkinson, A.C., Ishida, R., Nakauchi, H., and Yamazaki, S. (2020). Long-term ex vivo expansion of mouse hematopoietic stem cells. Nat Protoc *15*, 628-648. 10.1038/s41596-019-0263-2.
27. Jacobi, A.M., Rettig, G.R., Turk, R., Collingwood, M.A., Zeiner, S.A., Quadros, R.M., Harms, D.W., Bonthuis, P.J., Gregg, C., Ohtsuka, M., et al. (2017). Simplified CRISPR tools for efficient genome editing and streamlined protocols for their delivery into mammalian cells and mouse zygotes. Methods *121-122*, 16-28. 10.1016/j.ymeth.2017.03.021.
28. Cieśla, M., Ngoc, P.C.T., Cordero, E., Martinez Á, S., Morsing, M., Muthukumar, S., Beneventi, G., Madej, M., Munita, R., Jönsson, T., et al. (2021). Oncogenic translation directs spliceosome dynamics revealing an integral role for SF3A3 in breast cancer. Mol Cell *81*, 1453-1468.e1412. 10.1016/j.molcel.2021.01.034.
29. Kent, W.J., Sugnet, C.W., Furey, T.S., Roskin, K.M., Pringle, T.H., Zahler, A.M., and Haussler, D. (2002). The human genome browser at UCSC. Genome Res *12*, 996-1006. 10.1101/gr.229102.
30. Guzzi, N., Cieśla, M., Ngoc, P.C.T., Lang, S., Arora, S., Dimitriou, M., Pimková, K., Sommarin, M.N.E., Munita, R., Lubas, M., et al. (2018). Pseudouridylation of tRNA-Derived Fragments Steers Translational Control in Stem Cells. Cell *173*, 1204-1216.e1226. 10.1016/j.cell.2018.03.008.
31. Sagliocco, F.A., Moore, P.A., and Brown, A.J. (1996). Polysome analysis. Methods Mol Biol *53*, 297-311. 10.1385/0-89603-319-8:297.
32. Cieśla, M., Ngoc, P.C.T., Cordero, E., Martinez Á, S., Morsing, M., Muthukumar, S., Beneventi, G., Madej, M., Munita, R., Jönsson, T., et al. (2021). Oncogenic translation directs spliceosome dynamics revealing an integral role for SF3A3 in breast cancer. Mol Cell *81*, 1453-1468.e1412. 10.1016/j.molcel.2021.01.034.
33. Schmidt, K., Joyce, C.E., Buquicchio, F., Brown, A., Ritz, J., Distel, R.J., Yoon, C.H., and Novina, C.D. (2016). The lncRNA SLNCR1 Mediates Melanoma Invasion through a Conserved SRA1-like Region. Cell Rep *15*, 2025-2037. 10.1016/j.celrep.2016.04.018.
34. Tyanova, S., Temu, T., and Cox, J. (2016). The MaxQuant computational platform for mass spectrometry-based shotgun proteomics. Nat Protoc *11*, 2301-2319. 10.1038/nprot.2016.136.

35. UniProt: the Universal Protein Knowledgebase in 2023. (2023). Nucleic Acids Res *51*, D523-d531. 10.1093/nar/gkac1052.
36. Tyanova, S., Temu, T., Sinitcyn, P., Carlson, A., Hein, M.Y., Geiger, T., Mann, M., and Cox, J. (2016). The Perseus computational platform for comprehensive analysis of (prote)omics data. Nat Methods *13*, 731-740. 10.1038/nmeth.3901.
37. Roehr, J.T., Dieterich, C., and Reinert, K. (2017). Flexbar 3.0 - SIMD and multicore parallelization. Bioinformatics *33*, 2941-2942. 10.1093/bioinformatics/btx330.
38. Dobin, A., Davis, C.A., Schlesinger, F., Drenkow, J., Zaleski, C., Jha, S., Batut, P., Chaisson, M., and Gingeras, T.R. (2013). STAR: ultrafast universal RNA-seq aligner. Bioinformatics *29*, 15-21. 10.1093/bioinformatics/bts635.
39. Ramírez, F., Ryan, D.P., Grüning, B., Bhardwaj, V., Kilpert, F., Richter, A.S., Heyne, S., Dündar, F., and Manke, T. (2016). deepTools2: a next generation web server for deep-sequencing data analysis. Nucleic Acids Res *44*, W160-165. 10.1093/nar/gkw257.
40. Petfalski, E., Winz, M.L., Grelewska-Nowotko, K., Turowski, T.W., and Tollervey, D. (2025). Multiple mechanisms of termination modulate the dynamics of RNAPI transcription. Cell Rep *44*, 115325. 10.1016/j.celrep.2025.115325.
41. Rogalska, M.E., Mancini, E., Bonnal, S., Gohr, A., Dunyak, B.M., Arecco, N., Smith, P.G., Vaillancourt, F.H., and Valcárcel, J. (2024). Transcriptome-wide splicing network reveals specialized regulatory functions of the core spliceosome. Science *386*, 551-560. 10.1126/science.adn8105.
42. Jones, R.C., Karkanias, J., Krasnow, M.A., Pisco, A.O., Quake, S.R., Salzman, J., Yosef, N., Bulthaup, B., Brown, P., Harper, W., et al. (2022). The Tabula Sapiens: A multiple-organ, single-cell transcriptomic atlas of humans. Science *376*, eabl4896. 10.1126/science.abl4896.
43. Jiang, H., Lei, R., Ding, S.W., and Zhu, S. (2014). Skewer: a fast and accurate adapter trimmer for next-generation sequencing paired-end reads. BMC Bioinformatics *15*, 182. 10.1186/1471-2105-15-182.
44. Love, M.I., Huber, W., and Anders, S. (2014). Moderated estimation of fold change and dispersion for RNA-seq data with DESeq2. Genome Biol *15*, 550. 10.1186/s13059-014-0550-8.
45. Shen, S., Park, J.W., Lu, Z.X., Lin, L., Henry, M.D., Wu, Y.N., Zhou, Q., and Xing, Y. (2014). rMATS: robust and flexible detection of differential alternative splicing from replicate RNA-Seq data. Proc Natl Acad Sci U S A *111*, E5593-5601. 10.1073/pnas.1419161111.
46. Ray, D., Kazan, H., Cook, K.B., Weirauch, M.T., Najafabadi, H.S., Li, X., Gueroussov, S., Albu, M., Zheng, H., Yang, A., et al. (2013). A compendium of RNA-binding motifs for decoding gene regulation. Nature *499*, 172-177. 10.1038/nature12311.
47. Gohr, A., and Irimia, M. (2019). Matt: Unix tools for alternative splicing analysis. Bioinformatics *35*, 130-132. 10.1093/bioinformatics/bty606.
48. McGinnis, C.S., Patterson, D.M., Winkler, J., Conrad, D.N., Hein, M.Y., Srivastava, V., Hu, J.L., Murrow, L.M., Weissman, J.S., Werb, Z., et al. (2019). MULTI-seq: sample multiplexing for single-cell RNA sequencing using lipid-tagged indices. Nat Methods *16*, 619-626. 10.1038/s41592-019-0433-8.
49. Signer, R.A., Magee, J.A., Salic, A., and Morrison, S.J. (2014). Haematopoietic stem cells require a highly regulated protein synthesis rate. Nature *509*, 49-54. 10.1038/nature13035.
50. Guzzi, N., Muthukumar, S., Cieśla, M., Todisco, G., Ngoc, P.C.T., Madej, M., Munita, R., Fazio, S., Ekström, S., Mortera-Blanco, T., et al. (2022). Pseudouridine-modified tRNA fragments repress aberrant protein synthesis and predict leukaemic progression in myelodysplastic syndrome. Nat Cell Biol *24*, 299-306. 10.1038/s41556-022-00852-9.
51. Lee, S.C., and Abdel-Wahab, O. (2016). Therapeutic targeting of splicing in cancer. Nat Med *22*, 976-986. 10.1038/nm.4165.

52. Ramabadran, R., Wang, J.H., Reyes, J.M., Guzman, A.G., Gupta, S., Rosas, C., Brunetti, L., Gundry, M.C., Tovy, A., Long, H., et al. (2023). DNMT3A-coordinated splicing governs the stem state switch towards differentiation in embryonic and haematopoietic stem cells. Nat Cell Biol *25*, 528-539. 10.1038/s41556-023-01109-9.
53. Wang, H., Zhang, Z., Han, C., Jiang, P., Xu, J., Han, Y., Huang, D., Li, J., Zhou, J., Durnin, M., et al. (2025). SNORD113-114 cluster maintains haematopoietic stem cell self-renewal via orchestrating the translation machinery. Nat Cell Biol *27*, 246-261. 10.1038/s41556-024-01593-7.
54. Seita, J., Sahoo, D., Rossi, D.J., Bhattacharya, D., Serwold, T., Inlay, M.A., Ehrlich, L.I., Fathman, J.W., Dill, D.L., and Weissman, I.L. (2012). Gene Expression Commons: an open platform for absolute gene expression profiling. PLoS One *7*, e40321. 10.1371/journal.pone.0040321.
55. Liu, Z., Luyten, I., Bottomley, M.J., Messias, A.C., Houngninou-Molango, S., Sprangers, R., Zanier, K., Krämer, A., and Sattler, M. (2001). Structural basis for recognition of the intron branch site RNA by splicing factor 1. Science *294*, 1098-1102. 10.1126/science.1064719.
56. Leppek, K., Das, R., and Barna, M. (2018). Functional 5' UTR mRNA structures in eukaryotic translation regulation and how to find them. Nat Rev Mol Cell Biol *19*, 158-174. 10.1038/nrm.2017.103.
57. Hinnebusch, A.G. (2017). Structural Insights into the Mechanism of Scanning and Start Codon Recognition in Eukaryotic Translation Initiation. Trends Biochem Sci *42*, 589-611. 10.1016/j.tibs.2017.03.004.
58. Xia, T., Dai, X.Y., Sang, M.Y., Zhang, X., Xu, F., Wu, J., Shi, L., Wei, J.F., and Ding, Q. (2024). IGF2BP2 Drives Cell Cycle Progression in Triple-Negative Breast Cancer by Recruiting EIF4A1 to Promote the m6A-Modified CDK6 Translation Initiation Process. Adv Sci (Weinh) *11*, e2305142. 10.1002/advs.202305142.
59. Huang, H., Weng, H., Sun, W., Qin, X., Shi, H., Wu, H., Zhao, B.S., Mesquita, A., Liu, C., Yuan, C.L., et al. (2018). Recognition of RNA N(6)-methyladenosine by IGF2BP proteins enhances mRNA stability and translation. Nat Cell Biol *20*, 285-295. 10.1038/s41556-018-0045-z.
60. Huang, H., Weng, H., Sun, W., Qin, X., Shi, H., Wu, H., Zhao, B.S., Mesquita, A., Liu, C., Yuan, C.L., et al. (2018). Recognition of RNA N(6)-methyladenosine by IGF2BP proteins enhances mRNA stability and translation. Nat Cell Biol *20*, 285-295. 10.1038/s41556-018-0045-z.
61. Blokzijl-Franke, S., Ponsioen, B., Schulte-Merker, S., Herbomel, P., Kissa, K., Choorapoikayil, S., and den Hertog, J. (2021). Phosphatidylinositol-3 kinase signaling controls survival and stemness of hematopoietic stem and progenitor cells. Oncogene *40*, 2741-2755. 10.1038/s41388-021-01733-5.
62. Hemmati, S., Sinclair, T., Tong, M., Bartholdy, B., Okabe, R.O., Ames, K., Ostrodka, L., Haque, T., Kaur, I., Mills, T.S., et al. (2019). PI3 kinase alpha and delta promote hematopoietic stem cell activation. JCI Insight *5*. 10.1172/jci.insight.125832.
63. Piszczatowski, R.T., Bülow, H.E., and Steidl, U. (2024). Heparan sulfates and heparan sulfate proteoglycans in hematopoiesis. Blood *143*, 2571-2587. 10.1182/blood.2023022736.
64. Gupta, P., Oegema, T.R., Jr., Brazil, J.J., Dudek, A.Z., Slungaard, A., and Verfaillie, C.M. (1998). Structurally specific heparan sulfates support primitive human hematopoiesis by formation of a multimolecular stem cell niche. Blood *92*, 4641-4651.
65. Rich, I.N., Brackmann, I., Worthington-White, D., and Dewey, M.J. (1998). Activation of the sodium/hydrogen exchanger via the fibronectin-integrin pathway results in hematopoietic stimulation. J Cell Physiol *177*, 109-122. 10.1002/(sici)1097-4652(199810)177:1<109::Aid-jcp12>3.0.Co;2-8.
66. Pashos, A.R.S., Meyer, A.R., Bussey-Sutton, C., O'Connor, E.S., Coradin, M., Coulombe, M., Riemondy, K.A., Potlapelly, S., Strahl, B.D., Hansson, G.C., et al. (2025). H3K36 methylation regulates cell plasticity and regeneration in the intestinal epithelium. Nat Cell Biol *27*, 202-217. 10.1038/s41556-024-01580-y.

67. Chu, S.H., Chabon, J.R., Matovina, C.N., Minehart, J.C., Chen, B.R., Zhang, J., Kumar, V., Xiong, Y., Callen, E., Hung, P.J., et al. (2020). Loss of H3K36 Methyltransferase SETD2 Impairs V(D)J Recombination during Lymphoid Development. iScience *23*, 100941. 10.1016/j.isci.2020.100941.
68. Wang, Y., Xie, Z., Kutschera, E., Adams, J.I., Kadash-Edmondson, K.E., and Xing, Y. (2024). rMATS-turbo: an efficient and flexible computational tool for alternative splicing analysis of large-scale RNA-seq data. Nat Protoc *19*, 1083-1104. 10.1038/s41596-023-00944-2.
69. Guth, S., and Valcárcel, J. (2000). Kinetic role for mammalian SF1/BBP in spliceosome assembly and function after polypyrimidine tract recognition by U2AF. J Biol Chem *275*, 38059-38066. 10.1074/jbc.M001483200.
70. Arning, S., Grüter, P., Bilbe, G., and Krämer, A. (1996). Mammalian splicing factor SF1 is encoded by variant cDNAs and binds to RNA. Rna *2*, 794-810.
71. Heintz, C., Doktor, T.K., Lanjuin, A., Escoubas, C., Zhang, Y., Weir, H.J., Dutta, S., Silva-García, C.G., Bruun, G.H., Morantte, I., et al. (2017). Splicing factor 1 modulates dietary restriction and TORC1 pathway longevity in C. elegans. Nature *541*, 102-106. 10.1038/nature20789.
72. Dever, T.E. (2002). Gene-specific regulation by general translation factors. Cell *108*, 545-556. 10.1016/s0092-8674(02)00642-6.
73. Gebauer, F., and Hentze, M.W. (2004). Molecular mechanisms of translational control. Nat Rev Mol Cell Biol *5*, 827-835. 10.1038/nrm1488.
74. Farache, D., Antine, S.P., and Lee, A.S.Y. (2022). Moonlighting translation factors: multifunctionality drives diverse gene regulation. Trends Cell Biol *32*, 762-772. 10.1016/j.tcb.2022.03.006.
75. Jambor, H., Brunel, C., and Ephrussi, A. (2011). Dimerization of oskar 3' UTRs promotes hitchhiking for RNA localization in the Drosophila oocyte. Rna *17*, 2049-2057. 10.1261/rna.2686411.
76. Traunmüller, L., Schulz, J., Ortiz, R., Feng, H., Furlanis, E., Gomez, A.M., Schreiner, D., Bischofberger, J., Zhang, C., and Scheiffele, P. (2023). A cell-type-specific alternative splicing regulator shapes synapse properties in a trans-synaptic manner. Cell Rep *42*, 112173. 10.1016/j.celrep.2023.112173.
77. Zheng, S., and Black, D.L. (2013). Alternative pre-mRNA splicing in neurons: growing up and extending its reach. Trends Genet *29*, 442-448. 10.1016/j.tig.2013.04.003.
78. Masuda, A., Okamoto, T., Kawachi, T., Takeda, J.I., Hamaguchi, T., and Ohno, K. (2024). Blending and separating dynamics of RNA-binding proteins develop architectural splicing networks spreading throughout the nucleus. Mol Cell *84*, 2949-2965.e2910. 10.1016/j.molcel.2024.07.001.
79. Bhat, P., Chow, A., Emert, B., Ettlin, O., Quinodoz, S.A., Strehle, M., Takei, Y., Burr, A., Goronzy, I.N., Chen, A.W., et al. (2024). Genome organization around nuclear speckles drives mRNA splicing efficiency. Nature *629*, 1165-1173. 10.1038/s41586-024-07429-6.
80. Liu, Y., Elf, S.E., Miyata, Y., Sashida, G., Liu, Y., Huang, G., Di Giandomenico, S., Lee, J.M., Deblasio, A., Menendez, S., et al. (2009). p53 regulates hematopoietic stem cell quiescence. Cell Stem Cell *4*, 37-48. 10.1016/j.stem.2008.11.006.
81. Milyavsky, M., Gan, O.I., Trottier, M., Komosa, M., Tabach, O., Notta, F., Lechman, E., Hermans, K.G., Eppert, K., Konovalova, Z., et al. (2010). A distinctive DNA damage response in human hematopoietic stem cells reveals an apoptosis-independent role for p53 in self-renewal. Cell Stem Cell *7*, 186-197. 10.1016/j.stem.2010.05.016.

FIGURE LEGENDS

Figure 1 Post-transcriptional regulation of splicing factors during hematopoietic differentiation.

(A) Schematic shows the analysis pipeline: 'fingerprints' of splicing factor activity were inferred using gene expression signatures from knockdowns of 305 splicing factors[41], applied to the Tabula Sapiens single-cell atlas[42]. UMAP shows individual cell populations across human bone marrow, blood and lymph node tissues.

(B) Heatmaps show inferred splicing factor activity across tissues overlaid on Tabula Sapiens UMAP, grouped by core functional complexes (U1, U2, U5, U4/U6 and tri-snRNP). Negative enrichment indicates inferred high activity; positive enrichment indicates low inferred activity.

(C) Lollipop plots show differential enrichment for activities of inferred signatures of splicing factor families across hematopoietic stem cells (HSCs), hematopoietic precursor cells (HPCs) and B-cells.

(D) K-means clustering of mRNA-corrected splicing factor activity scores across hematopoietic subsets from the Tabula Sapiens single-cell transcriptomic dataset[42], revealing 16 distinct regulatory clusters. Cell populations are ordered to reflect the approximate progression of hematopoietic differentiation rather than a formal pseudotime inference.

(E) Venn diagram showing overlap in post-transcriptionally regulated splicing factors between hematopoietic stem and progenitor cells (HSPCs), myeloid, lymphoid, and erythroid subsets. See also Figure S1.

Figure 2 Dynamics in early acting splicing factors define differentiation trajectories of hematopoietic stem cells

(A) Violin plot shows relative expression of 39 splicing factors detected in sequencing of ribosome-protected footprints in blood subpopulations from[53]. Data are normalized and statistically compared to expression in long-term (LT) HSCs. ***p<0.001; **p<0.01; *p<0.05 (ANOVA).

(B) Schematic illustrates an experiment designed to define the dynamics of first-stage splicing factors along the hematopoietic differentiation trajectory. BP – branch point; HSC – hematopoietic stem cell; MPP – multipotent progenitor; GMLP – granulocyte-monocyte-lymphoid progenitor; MyP – myeloid progenitors; lymphoid – lymphoid cells; myeloid – myeloid cells.

(C) Graphs show quantification of RNA and protein levels of core splicing factors from the branch point recognition complex along the hematopoietic differentiation trajectory. Lines and shaded areas show, respectively, mean expression ± SD. (n = 4-5).

(D) Representative flow cytometry histograms showing protein expression of Sf1 and Sf3a3 in the indicated blood cell populations.

(E) Reducing the levels of core splicing factors specifically reduces expansion and differentiation rates *ex vivo*. Schematic shows the outline of an experiment to define impact of knock-down with RNA interference of individual splicing factors from **(C)** on expansion and stemness at day 8 of *ex vivo* cultured hematopoietic stem and progenitor cells (HSPCs). Graphs show the cell number (top) and percentage of $CD150^+$ $Lineage^-$ $Sca\text{-}1^+$ $cKIT^+$ early blood progenitors (bottom) ± SD. ****p<0.0001; ***p<0.001; **p<0.01; *p<0.05 (one-way ANOVA). (n = 4-6).

(F) Representative FACS plots show the distribution of HSPC populations in primary *ex vivo* expanded $cKIT^+$ hematopoietic cells transfected with control (siCTRL) and Sf1-targeting (siSf1) short interfering RNA. Bar graph shows the distribution of $CD150^+$ LSK population between control (siCTRL) and Sf1-knock down (siSf1) HSPCs. **p<0.01 (t test, siCTRL vs. siSf1). (n = 5-6).

(G) Representative images of methylcellulose plates from colony-forming unit (CFU) assay show a decrease in differentiation potential upon Sf1 downregulation (siSf1). Graph shows quantification of colony number ± SD in control (siCTRL) and Sf1 knock down (siSf1) samples. **p<0.01 (t test) (n = 4).

(H) Representative images show changes in morphology assessed by May-Grünwald-Giemsa (MGG) staining.

See also Figure S2.

Figure 3 Translation of Sf1 is Controlled via a Structured Stem-Loop 5' UTR Regulatory Element

(A) Schematic depicts UCSC GRCm39/mm39 genome browser track for evolutionary conservation within the genomic region corresponding to the Sf1 5′ UTR.

(B) Predicted secondary structure of 398-nt Sf1 5′ UTR determined with RNAfold. Nucleotides are colored with MFE reactivities, and size-coded based on the evolutionary conservation scores from the UCSC genome browser.

(C – **E)** Stem-loop2 (SL2) structure within the 51–100 nt region of Sf1 5′ UTR drives translation control. Schematic depicts the monocistronic translational reporter employed to measure the activity of the 5′ UTR *Sf1* in murine NIH3T3 fibroblasts (24 h) **(C).** Graph shows fold change (FC) mean FLuc activity normalized to the FLuc RNA expression and relative to the full-length, wild-type (WT) *Sf1* 5′ UTR ± SD. $^{**}p < 0.01$ (one-way ANOVA) (n = 4-8) **(D).** Reporter assay using transverse mutants of stem loops 2 and 3 (SL2/3) of *Sf1* 5′ UTR (top). Graph shows $\log_2$ -transformed fold change (FC) mean FLuc activity normalized to the full-length, WT *Sf1* 5′ UTR ± SD. $^{**}p < 0.01$; $^{*}p<0.05$ (one-way ANOVA) (n = 4-10) **(E).**

(F) Representative protein analysis with quantification ± SD and graph showing of mRNA levels ± SD illustrate decreased Sf1 protein, but not mRNA levels in CRISPR-Cas9 edited murine fibroblasts NIH3T3 lacking 51–200 nt region of 5′ UTR (n = 2-5).

(G) Representative protein analysis and graph showing quantification ± SD of mRNA levels illustrate decreased Sf1 protein, but not mRNA, levels in 5′ UTR del(51-100) HSPCs (n = 7-8).

(H) Polysomal analysis of Sf1 mRNA in control and Sf1 del(51-100) HSPCs. The polysome profile (grey shading) indicates relative absorbance at 254 nm. Graph shows normalized mean *Sf1* mRNA abundance across polysomal fractions in control and del(51-100) HSPCs, presented as mean ± SD. $^{*}p < 0.05$ (t test). n = 4 independent mice per condition.

See also Figure S3.

Figure 4 Sf1 translation requires a *cis*-acting 5′UTR stem-loop and Igf2bp2-mediated regulation.

(A) Schematic shows strategy for quantitative proteomic analysis of Sf1 5′ UTR RNA pulldowns in NIH3T3 cells. Scatter plot shows proteins specifically enriched on the WT 5′ UTR compared to del(51-100) and control background identified by tandem mass tag (TMT)-labeled mass spectrometry. Igf2bp2 emerged as a prominent candidate that selectively binds the WT element.

(B) CLIP-seq traces show binding of Igf2bp2 across the *Sf1* transcript (top) in NIH3T3 murine fibroblasts (n = 2). Bottom: focus on the 5' UTR region of the Sf1 transcript.

(C) Bar graph shows results of luciferase reporter assays using constructs harboring the WT *Sf1* 5′UTR or mutant variants (del(51-100) and SL2.1 disrupting the stem-loop structure). Knockdown of Igf2bp2 selectively reduced translation of the WT reporter but not the mutant variants. **p<0.01, *p<0.05 (one-way ANOVA) (n = 4).

(D) Representative immunoblot analysis of Sf1 protein levels following Igf2bp2 knockdown in NIH3T3 murine fibroblasts. Bar graph shows quantification of protein levels ± siIgf2bp2 in NIH3T3 cells, ***p<0.001 (t test) (n = 6).

(E) Representative immunoblot analysis of Sf1 protein levels following Igf2bp2 knockdown in *in vitro* expanded primary murine hematopoietic stem and progenitor cells (HSPCs, cKIT$^+$ fraction).

(F) Representative polysome profiles of NIH3T3 cells following Igf2bp2 knockdown. Inset shows the level of Igf2bp2 knock down in control and Igf2bp2-depleted cells.

(G) Distribution of Sf1 transcript across polysomal fractions. Sf1 transcripts shifted from heavy to light polysome fractions, consistent with impaired translational efficiency. **p<0.01 (t test) (n = 3). Graph shows normalized mean Sf1 mRNA abundance in each polysomal fraction ± SD in siCTRL and siIgf2bp2 NIH3T3. Bar graph shows quantification of Sf1 mRNA levels ± siIgf2bp2 in NIH3T3 cells (n = 3).

(H) Schematic shows the outline of an experiment to define the impact of knock-down with RNA interference of Igf2bp2 (siIgf2bp2) on CD150+ LSK HSPCs. Representative FACS plots show the distribution of HSPC populations in primary *ex vivo* expanded cKIT$^+$ hematopoietic cells transfected with control (siCTRL) or Igf2bp2-targeting (siIgf2bp2) short interfering RNA. Graph shows quantification of CD150$^+$ LSK HSPCs between siCTRL) and Igf2bp siIgf2bp2 HSPCs. *p<0.05 (t test) (n = 3).

See also Figure S4.

Figure 5 Loss of Translational Control of Sf1 Alters HSC Fate and Enhances Stem Cell Potential

(A) UMAP embedding of 41,515 *ex vivo* expanded murine HSPCs. The UMAP embedding and Leiden clustering were performed on the gene expression modality from the single-cell RNA-seq dataset. Individual cells are labeled based on of their cluster identity and size-coded according to the proximity to the closest neighbors.

(B) CellRadar plots show transcriptomic signatures of 7 identified clusters corresponding to myeloid, lymphoid, erythroid, and stem (HSPCs) signatures.

(C) UMAP plots show the distribution of HSPCs by sample type. Control (CTRL) density is shown in grey and del(51-100) density in blue. Stacked bar charts show the proportional distribution of CTRL and del(51-100) samples by cell cluster from **(B)**.

(D) Dot plot shows the average expression of the top-most enriched and depleted marker genes of del(51-100) in individual clusters of *ex vivo* expanded HSPCs. The size of dots represents the $\log_{10}$-transformed p-value, color encodes the $\log_2$-transformed fold change expression between del(51-100) and control cells. GO: Molecular Function (MF) ontologies for marker genes of del(51-100)-enriched 'ST-HSC' (cluster 2) and 'MkP/erythroid' (cluster 4) are depicted.

(E) CellRadar plot shows transcriptomic profiles of control and *del(51-100)* HSPCs.

(F) Schematic shows experimental strategy to evaluate differentiation potential and replating capacity between control (CTRL) and *del(51-100)* HSPCs. Stacked bar plot shows distribution of colonies (CFU-GM, CFU-GEMM and BFU-E) between CTRL and del(51-100) HSPCs. ****p<0.0001; ***p<0.001 (One-way ANOVA, CTRL vs. del(51-100) HSPCs), (n = 3).

(G) Graph shows number of colonies upon replating of 1000 control (CTRL) and del(51-100*)* HSPCs. ***p<0.001 (t test, CTRL vs. del(51-100) HSPCs), (n = 6).

(H – J) Loss of translational control of Sf1 increases *in vivo* outputs from murine HSPCs. Schematic depicts the experimental approach for the transplantation assay to test for the *in vivo* fitness of control (CTRL) and del(51-100) *ex vivo* expanded HSPCs with competition of whole bone marrow (WBM) cells. **(H)**. Graph shows total chimerism in peripheral blood (PB) in control (n = 4-5) and Sf1 del(51-100) (n = 7) HSPC-transplanted recipient mice, presented as mean ± SEM. Statistical significance was assessed using two-way ANOVA (*p < 0.05, ***p < 0.001, ****p < 0.0001) **(I)**. Graph shows the total chimerism in bone marrow (BM) 16 weeks after transplantation in control (n = 4) and del(51-100) (n = 7) HSPC-transplanted animals ± SEM. *p<0.05 (t test) (**J,** *top*). Graph shows distribution of cells from lineage positive (LIN+), lineage negative, Sca-1 positive, cKIT positive (LSKs), lineage negative, Sca-1 negative, cKIT

positive (myeloid precursors - MyPs), and lineage negative, cKIT-negative (cKIT-) fractions (**J,** *bottom*).

(K) Schematic shows the experimental setup to study the effect of SF1-knockdown (siSF1) in human hematopoietic stem and precursor cells (HSPCs, $CD34^+$) subjected to expansion and erythroid differentiation phase.

(L) Graph shows the expansion of human HSPCs after expansion (week 1) and erythroid differentiation (weeks 2-3). ***p<0.001; **p<0.01; *p<0.05; (One-way ANOVA, siCTRL vs. siSF1 human HSPCs), (n = 3).

See also Figure S5 and Tables S2, S3 and S4.

Figure 6 Sf1 Translation Determines Alternative Splicing to switch 5' UTR Isoforms of mRNAs Encoding Hematopoietic and Genome Integrity Regulators.

(A) Loss of *Sf1* translation control affects alternative splicing events (ASEs) in HSPCs. Left: Experimental setup used to capture splicing changes in *ex vivo* expanded control (CTRL) and del(51-100) HSPCs. Right: Volcano plot showing percentage spliced-in (PSI) values for individual ASEs. Significantly increased (red, n = 1932) and decreased (blue, n = 1940) ASEs in Sf1 del(51-100) are highlighted (*n* = 4).

(B) Pie charts illustrating the number of skipped exons (SE), mutually exclusive exons (MXE), alternative 3′ splice sites (A3SS), alternative 5′ splice sites (A5SS), and retained introns (RI) in del(51-100) HSPCs.

(C) Gene Ontology (GO) analysis showing enriched (top) and depleted (bottom) GO categories among significantly skipped exons (SE) in del(51-100) cells.

(D) Bubble plot showing cumulative splicing change in significant ($p<0.05$, t test) DNA damage response-related mRNAs across splicing events.

(E) Pie charts showing increased localization of significantly skipped exon events in del(51-100) HSPCs within the specific regions of regulated transcripts among all and GO:DNA repair related mRNAs.

(F) Polysome analysis of Sf1-regulated Mbtps1 mRNA in control and Sf1 del(51–100) HSPCs. Graphs show normalized mean of *Mbtps1* mRNA abundance across polysomal fractions in control and del(51–100) HSPCs, presented as mean ± SD (n = 4 independent mice per condition). Mbtps1 is shown as a representative DNA damage response transcript identified among alternatively spliced genes with altered untranslated region architecture. Inset shows a representative isoform-specific PCR detecting the skipping of the 5' UTR-positioned exon 2.

(G) Immunofluorescence staining of DNA damage lesions using γH2AX antibody in CTRL and del(51-100) fibroblasts. Graphs show the quantification of $\gamma H2AX^{+}$ foci (n = 2).

(H) Pie charts illustrating the number of skipped exons (SE), mutually exclusive exons (MXE), alternative 3′ splice sites (A3SS), alternative 5′ splice sites (A5SS), and retained introns (RI) in siSF1 human HSPCs.

(I) Scatter plot shows the relation between alternative splicing and gene expression in siSF1 human HSPCs. Selected top genes with significant changes in expression and splicing are shown.

(J) Venn diagram shows significant overlap between human and murine HSPCs alternative splicing datasets.

(K) Gene Ontology (GO) analysis showing top GO categories among significantly skipped exons (SE) in siSF1 human HSPCs.

965 See also Figure S6 and Tables S5 and S6.

Figure 1

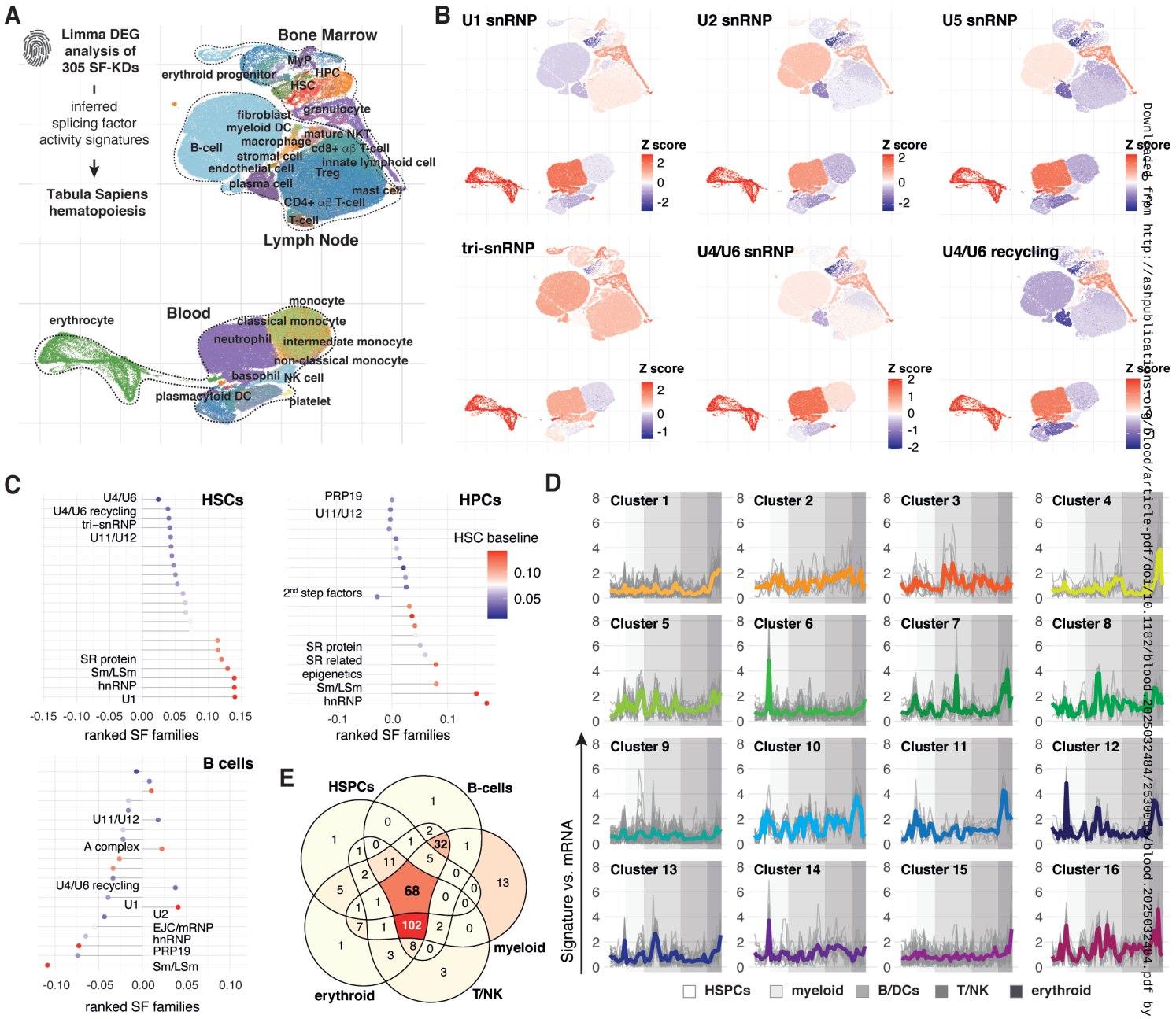

Figure 2

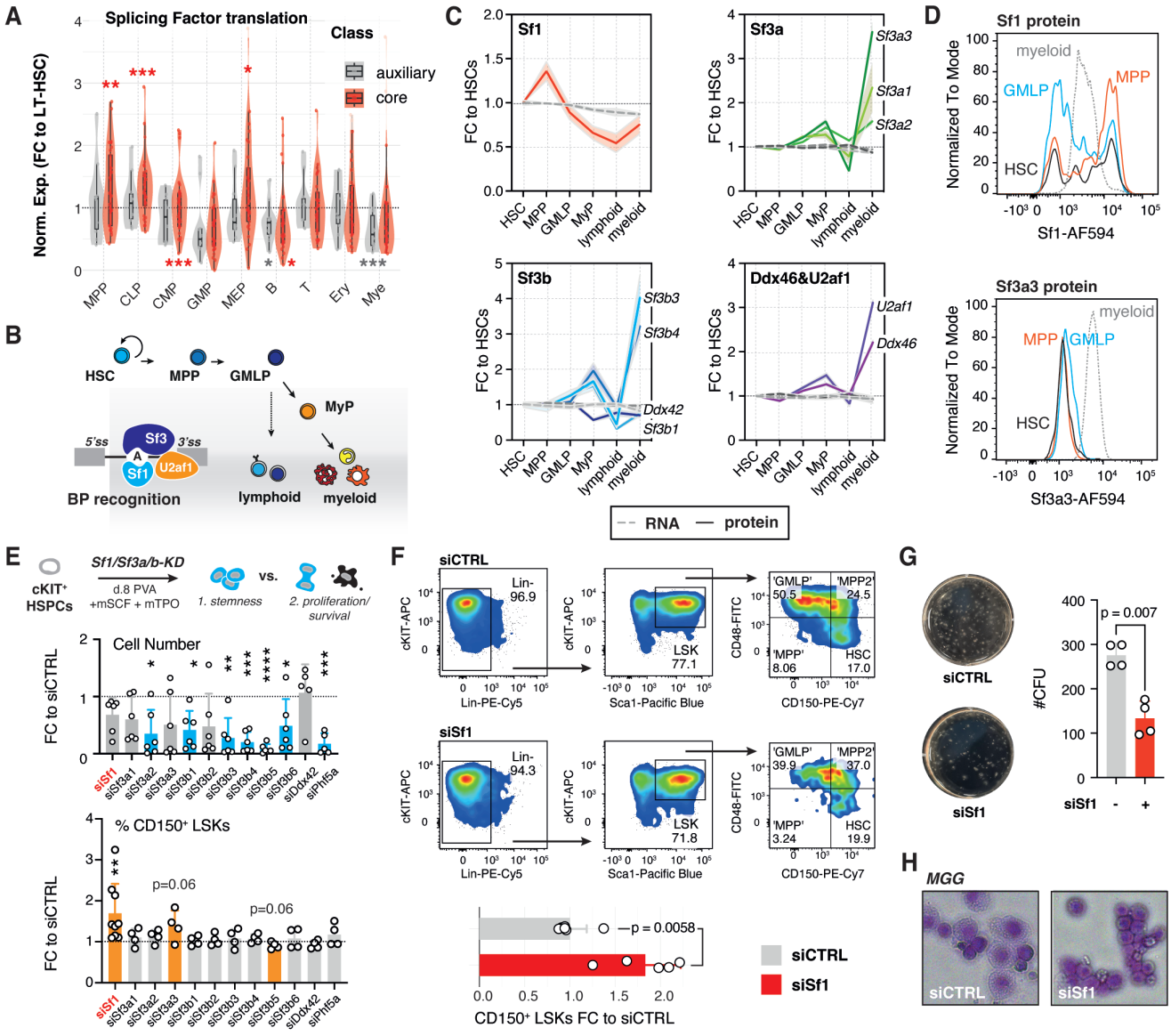

Figure 3

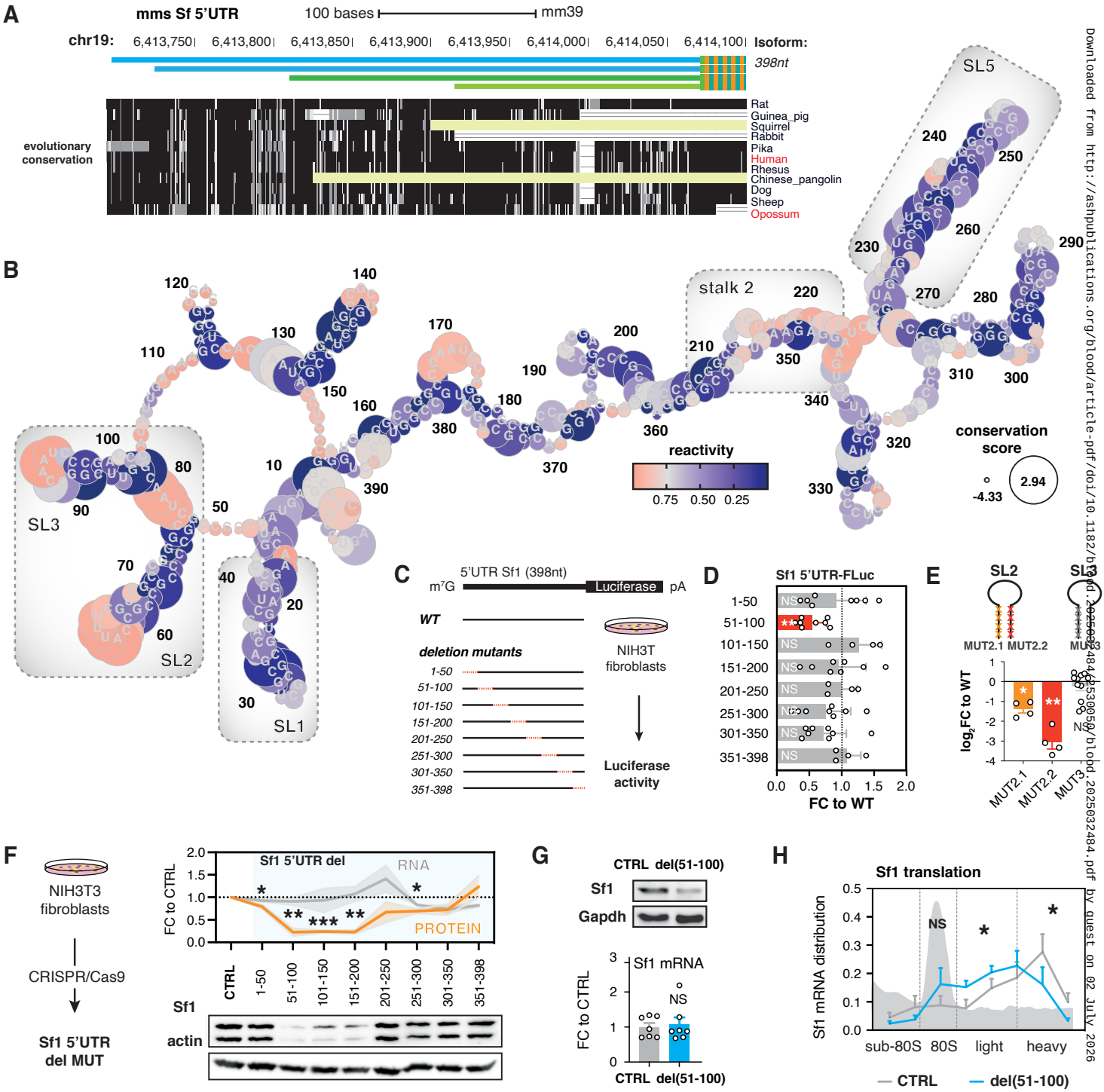

Figure 4

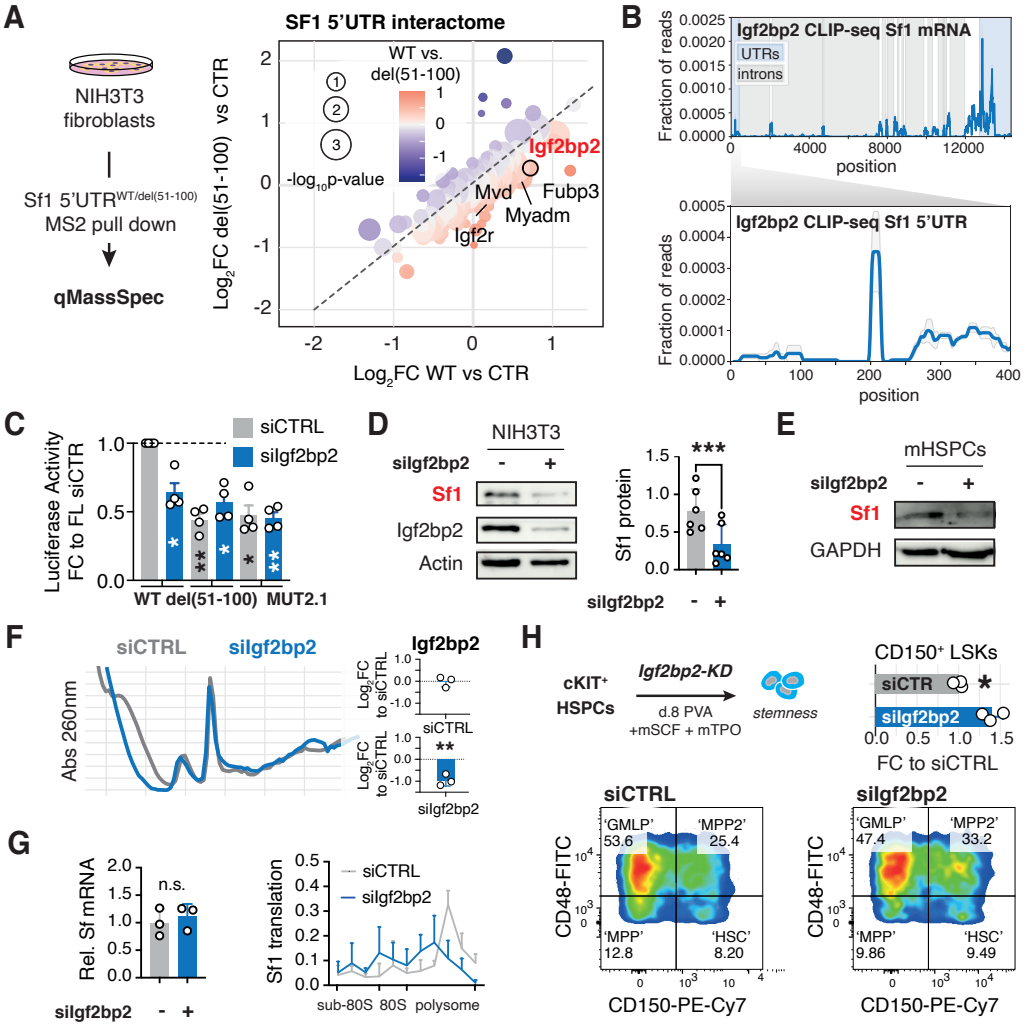

Figure 5

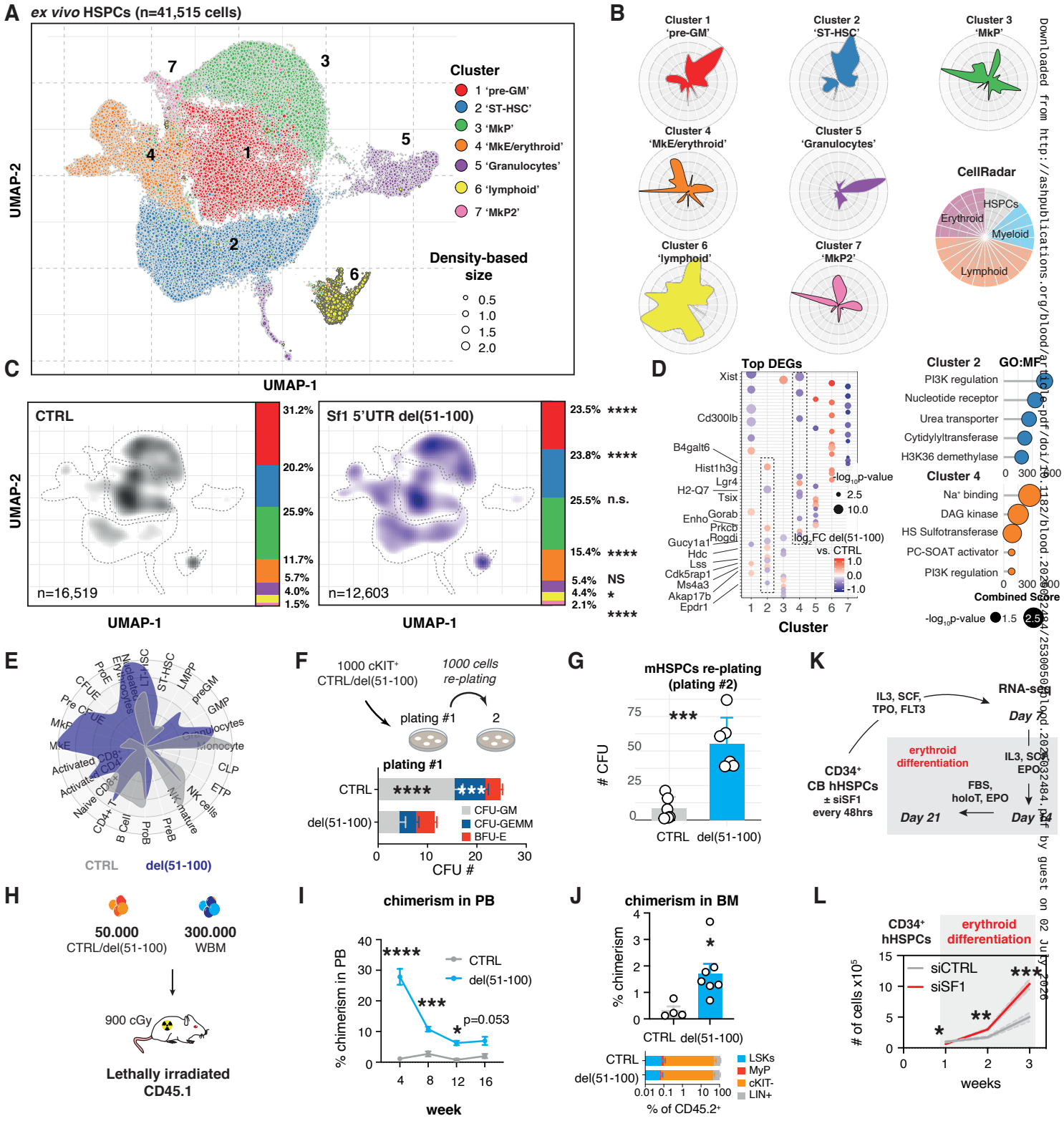

Figure 6